CRYSTAL GROWTH & DESIGN

Article

pubs.acs.org/crystal

The Formation of Hydrogen-Bond Facilitated Salts with Tunable Optical Properties: An Experimental and Theoretical Study of 2,4,5-Triphenylimidazole

Dongpeng Yan,*[,†] Bhavnita Patel,[‡] Amit Delori,[‡] William Jones,[‡] and Xue Duan[†]

[†]State Key Laboratory of Chemical Resource Engineering, Beijing University of Chemical Technology, Beijing, 100029, P. R. China

[‡]Department of Chemistry, University of Cambridge, Lensfield Road, Cambridge CB2 1EW, U. K.

Supporting Information

ABSTRACT: Adjusting and modifying the optical properties of organic fluorophores are of importance for the development of the next generation of luminescent materials. Herein, we report the tunable fluorescence of 2,4,5-triphenylimidazole (TPI) chromophore by the formation of multicomponent crystals with the supramolecular building blocks, 4-bromotetrafluorobenzene carboxylic acid and tetrafluorosuccinic acid, by means of hydrogen bonding. A change in packing fashions between two adjacent TPI molecules is observed from a staggered pattern in the pure TPI crystal to an antisymmetric parallel arrangement in the multicomponent crystals. Moreover, the obtained organic salts show red-shift emission and enhanced fluorescence lifetime compared with the pure TPI crystal. Periodic density functional theoretical (DFT) calculations suggest that the introduction of the coformers can influence the energy level structures and orbital distributions of the TPI chromophore in the multicomponent crystals. Therefore, by the combination of experimental and theoretical studies on the multicomponent organic solids, this work not only reports the supramolecular assembly of new types of photoactive solid-state materials but also provides a detailed understanding of the electronic structures of the luminescent materials.

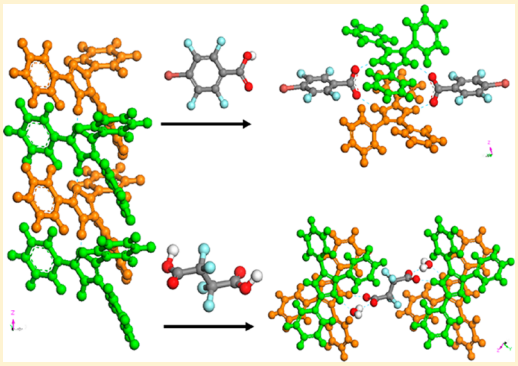

1. INTRODUCTION

Organic solid-state fluorescent materials have recently received considerable attention, due to their extensive applications in the optoelectronic fields of light-emitting diodes,[1] lasers,[2] solar cells,[3] and fluorescent sensors.[4] In views of fundamental studies and practical applications, the development of new solid-state multicomponent crystals of chromophores[5] based on supramolecular architecture is important to extend the type and application field of fluorescent materials and to complement organic synthetic chemistry. Moreover, by rational selection and design of the interaction between the components (supramolecular synthons),[6] the interaction mode, stacking states, and molecular recognition fashions between the assembled building blocks in the solid state can be modulated and controlled, which can further tailor the photophysical properties of the resulted organic solid-state suparmolecular materials.[7] However, to date, examples of multicomponent organic solids organized from two or more assembled units with tunable fluorescence are still limited compared with those of the polymorphism-dependent emission,[4g,h] probably because the cocrystallization is relatively difficult particularly when the components have very different solubilities.[6c] In addition, the detailed electronic structure and interaction fashion (such as energy/electronic transfer) between components within multicomponent crystals are seldom discussed.

2,4,5-Triphenylimidazole (TPI, Scheme 1A) is a typical fluorescent dye, which is well documented as a model system for the study of organic solid-state luminescence.[8] TPI contains a dicoordinate nitrogen atom, which can potentially build complexes assembled by hydrogen bonds with a molecule containing hydrogen-bond donor, such as a carboxylic acid. By the use of such a design strategy, we have herein developed two new types of TPI-based multicomponent crystal systems using liquid-assisted grinding (LAG) method,[9] and such method has been demonstrated to be able to overcome different solubilities between the components.[9b] Two representative compounds (BTFB (Scheme 1B) and TFS (Scheme 1C)) without visible fluorescence were chosen as the coformers with TPI. The obtained products show different light-emission properties (such as emission wavelength, fluorescence lifetime, and photoluminescence quantum yield (PLQY)) compared to those of the pure TPI organic solid. Detailed structures and interaction fashions between two components in the as-obtained multicomponent crystals were further characterized and analyzed by single crystal X-ray diffraction, solid-state NMR, differential scanning calorimetry, and thermogravimetric

Received: October 11, 2012
Revised: November 17, 2012
Published: December 5, 2012

Scheme 1. Chemical Structures of the Chromophore Molecule (A, 2,4,5-Triphenylimidazole (TPI)) and Coformers (B, 4-Bromotetrafluorobenzoic Acid (BTFB); C, Tetrafluorosuccinic Acid (TFS))

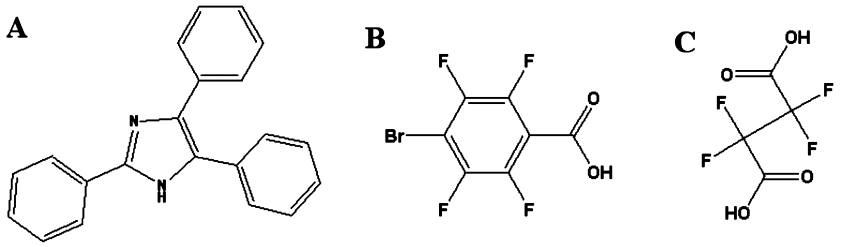

analysis. Moreover, periodic density functional theoretical (DFT) calculations were performed to explore detained electronic structures of the multicomponent crystals, to show the differences in energy level structures and orbital distributions of the TPI chromophore in the organic solids, which may in turn influence the photoexcitation/emission process. Therefore, by virtue of combining experimental and computational methods on the multicomponent luminescent systems, this work not only confirms that the construction of multicomponent crystals can serve as a facile way to tune the luminescent properties of an organic fluorescent dye through rational control of the interaction and arrangement fashions of chromophores within the crystal structures, but also provides a deep insight into how different coformers influence the electronic structures in these multicomponent crystals.

2. EXPERIMENTAL SECTION

2.1. Reagents. 2,4,5-Triphenylimidazole (TPI, **A**), 4-bromotetrafluorobenzoic acid (BTFB, **B**), and tetrafluorosuccinic acid (TFS, **C**) were purchased from Sigma Chemical Co. Ltd. and used without further purification.

2.2. Preparation of the Multicomponent Systems. In typical liquid-assisted grinding (LAG) experiments, 40 μL of a 3:1 (v/v) chloroform/water mixture was added to 200 mg of a solid reactant mixture (**A** + **B**; **A** + **C**) with the initial ratio of the two compositions of 1:1 (**A**:**B**) and 2:1 (**A**:**C**), respectively. The mixtures were ground for 30 min in a Retsch Mixer Mill MM200 mill at a frequency of 30 Hz using stainless steel jars (15 mL) and balls. In standard experiments, two stainless steel balls of 7 mm diameter (1.4 g) were used for grinding. Single crystals were obtained by adding 50 mL of chloroform solutions to the LAG products, which was allowed to evaporate over a period of one week.

2.3. Instrumentation. Characterization of solid materials using powder X-ray diffraction was conducted on an X-Pert PRO MPD powder X-ray diffractometer, using nickel-filtered Cu Kα radiation (1.54 Å) generated at 40 kV and 40 mA with a scanning rate of 10°/min, and a 2θ angle ranging from 3 to 50°. Single crystal X-ray diffraction data were collected for salts **A.B** and **2A.C(H$_2$O)** on a Nonius Kappa CCD diffractometer equipped with a graphite monochromator and an Oxford cryostream, using Mo Kα radiation. Differential scanning calorimetry (DSC) thermograms were measured on a DSC822e calorimeter under nitrogen with a heating rate of 10 °C/min. Thermogravimetric analysis (TGA) was conducted on TGA/SDTA851e thermobalance with a heating rate of 10 °C/min. The solid-state fluorescence spectra were performed on RF-5301PC fluorospectrophotometer, and the width of both the excitation and emission slit was 3 nm. The fluorescence decays were measured using a LifeSpec-ps spectrometer, and the lifetimes were calculated with the F900 Edinburgh instruments software. Photoluminescence quantum yield (PLQY) was measured using an HORIBA Jobin-Yvon FluoroMax-4 spectrofluorimeter, equipped with an F-3018 integrating sphere. Solid-state cross-polarization/magic angle spinning (CP/MAS) ^{13}C and ^{15}N nuclear magnetic resonance (NMR) spectra was recorded by Bruker BioSpin AV 300 MHz at 20 °C with a 4 mm rotor spinning at 5 kHz under a static magnetic field of 9.4 T. Morphologies of the crystal and powder samples were investigated by using a scanning electron microscope (SEM Zeiss Supra 55) with the accelerating voltage of 20 kV and an Olympus U-RFLT50 fluorescence microscope. Periodic density functional theory (DFT) calculations were performed using the Dmol3[10] module in the Material Studio software package.[11] The molecular structure of **A** and the single crystal structures of **A**, **A.B**, and **2A.C(H$_2$O)** were selected as the initial models, which were optimized by the Perdew–Wang (PW91)[12] generalized gradient approximation (GGA) method with the double numerical basis sets plus polarization function (DNP). The SCF convergence criterion was within 1.0×10^{-5} hartree/atom, and the convergence criterion of structure optimization was 1.0×10^{-3} hartree/bohr. The Brillouin zone (BZ) was sampled by 1 × 1 × 1 *k*-points, and test calculations revealed that an increased number of *k*-points does not influence the results.

2.4. Single Crystal Structures. Crystal data for **A.B** (CCDC: 900559) and **2A.C(H$_2$O)** (CCDC: 900560) are tabulated in Table 1.

Table 1. Crystal Structure Data for A.B and 2A.C(H$_2$O)

salts	A.B	2A.C(H$_2$O)
mol formula	$C_{28}H_{17}BrF_4N_2O_2$,	$C_{46}H_{38}F_4N_4O_6$
mol wt	569.35	818.80
color/shape	colorless/block	colorless/block
size (mm^3)	0.28 × 0.28 × 0.14	0.23× 0.21× 0.07
cryst syst	monoclinic	triclinic
space group	$P2(1)/c$	$P\bar{1}$
a (Å)	8.1916(1)	8.6090(1)
b (Å)	23.5372(5)	10.7972(2)
c (Å)	12.5644(3)	12.1225(2)
α (deg)	90.00	109.500(1)
β (deg)	104.577(1)	109.517(1)
γ (deg)	90.00	94.035(1)
V (Å^3)	2344.53(8)	979.96(3)
Z	4	1
D_c (g/cm^3,)	1.613	1.387
R_1 ($I > 2\sigma(I)$)	0.0512	0.0481
wR_2	0.1049	0.1030
GOF	1.022	1.031

3. RESULTS AND DISCUSSION

3.1. The Formation of Multicomponent Crystals. The new types of multicomponent crystals were synthesized by employing the liquid-assisted grinding (LAG) method.[9] Powder X-ray diffraction (PXRD) patterns of the as-prepared salts (1, **A** + **B**; 2, 2**A** + **C**), TPI, and the coformer precursors are shown in Figure 1. It can be observed that the PXRD patterns of the as-prepared multicomponent products are different from that of pure TPI (sample **A**) and its coformer precursors, demonstrating that new compositions have formed. Upon crystallization from chloroform, the transparent single

dx.doi.org/10.1021/cg3014927 | Cryst. Growth Des. 2013, 13, 333–340

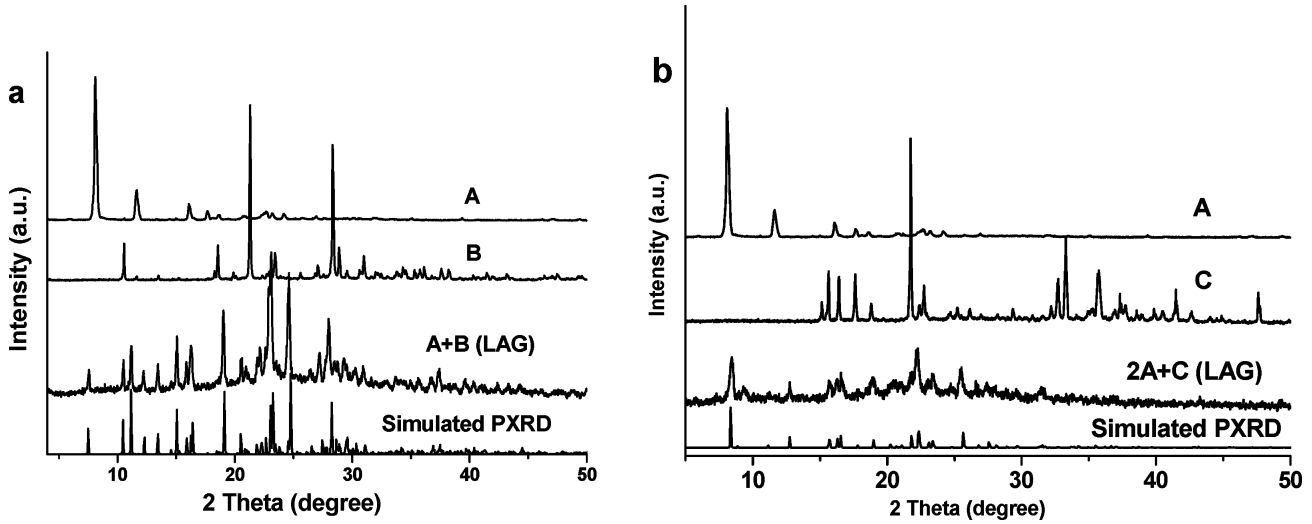

Figure 1. Powder XRD profiles of the multicomponent crystals (a) **A.B** and (b) **2A.C**(H_2O) and their assembled precursors, and simulated XRD from single crystal results respectively; **A**, 2,4,5-triphenylimidazole (TPI), and its coformer compounds **B**, 4-bromotetrafluorobenzene carboxylic acid (BTFB), and **C**, tetrafluorosuccinic acid (TFS).

Scheme 2. Crystal Structures of the Pure TPI and TPI-Based Multicomponent Crystals (A.B and 2A.C(H_2O))

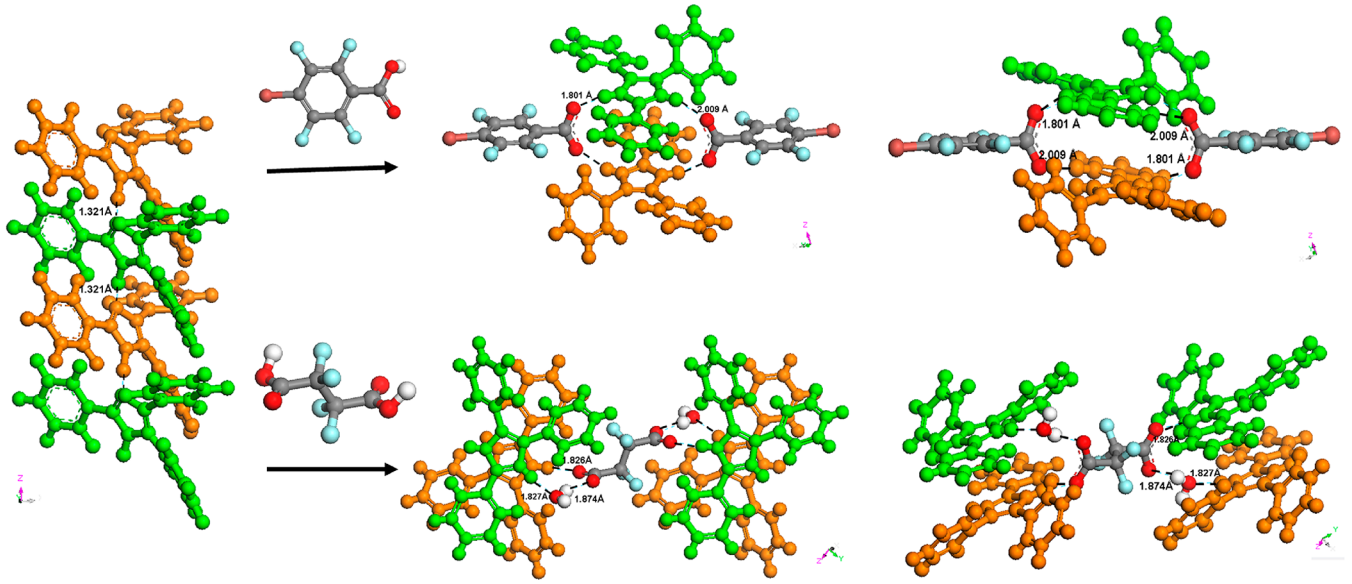

crystals of two complex systems can be obtained; the morphologies of the crystals as well as their LAG powder products are shown in Figure S1 in the Supporting Information. X-ray single crystal diffraction measurements were performed on the single crystal samples to obtain detailed crystal structures of the TPI-containing complex samples. The structures solved from the diffraction data confirm that these new members of TPI-containing multicomponent crystals are assembled by the hydrogen bond interaction between the dicoordinate nitrogen atom in TPI and carboxylic acid groups in the coformers with 1:1 (**A.B**) or 2:1 (**2A.C**) ratio, which is consistent with the initial design principle for the formation of the multicomponent crystals. The PXRD patterns are also consistent with the powder patterns simulated from the single crystal structures (Figure 1), illustrating a high purity of the obtained multicomponent powder samples formed by the LAG method. This further demonstrates that the LAG method can serve as an alternative crystallization technique for the rapid formation of large scale of multicomponent organic solids compared with the typical solution process.

Based on the single crystal diffraction results, we can further compare the differences in the assembled fashions between these crystal samples. In the crystal structure of **A** (Scheme 2), the molecules exhibit a staggered pattern assembled with the aid of the N−H···N hydrogen bonding between two adjacent TPI molecules. Upon formation of the **A.B** multicomponent crystal, proton transfer occurs from the carboxylic acid in **B** to the dicoordinate nitrogen atom of TPI, i.e., an ionic salt forms within the **A.B** crystal. Moreover, the TPI molecule shows an antisymmetric parallel arrangement assembled by the N−H···O hydrogen-bonding between **A** and **B**, which further organizes into an $R^4_4(16)$ dimeric motif.[13] Proton transfer was also observed in the **2A.C** system. The stacking fashion of TPI in **2A.C** is similar to that found in the **A.B** system. Three types of hydrogen bonds form between the **A** and H_2O (N−H···O), **C** and H_2O (O−H···O), and **A** and **C** (N−H···O), as shown in

dx.doi.org/10.1021/cg3014927 | *Cryst. Growth Des.* 2013, 13, 333−340

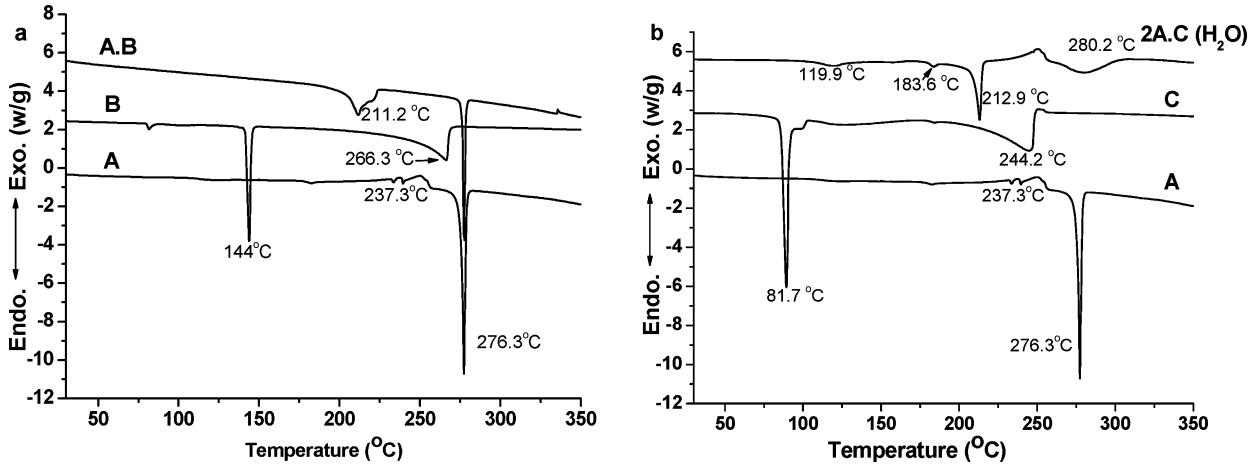

Figure 2. DSC profiles of the salts **A.B** and **2A.C**(H_2O) and their coformer precursors.

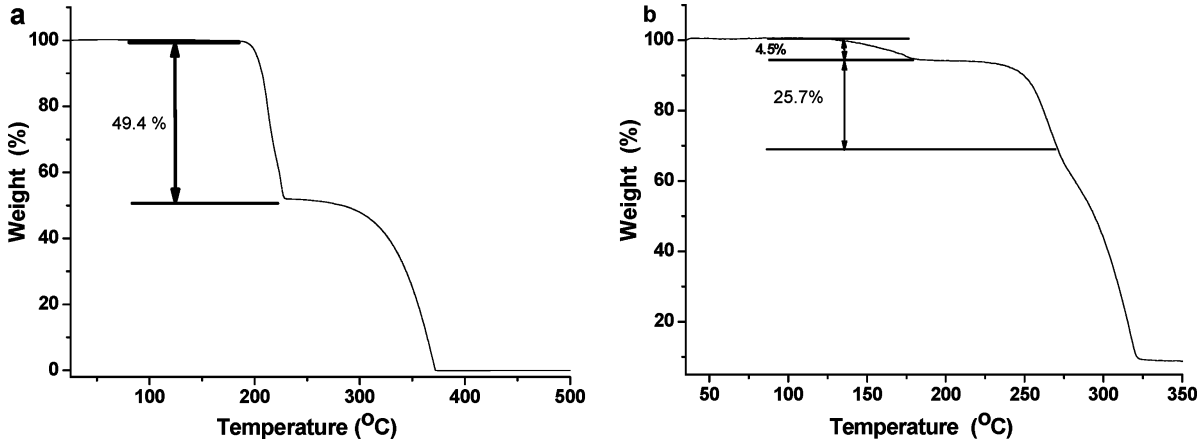

Figure 3. TGA profiles of the salts **A.B** and **2A.C**(H_2O) and their coformer precursors.

Scheme 2. Therefore, by the formation of hydrogen-bonding assembly of multicomponent organic crystals, the stacking and interaction fashions between the TPI chromophore were altered. The occurrence of H_2O molecule as guest within the **2A.C** host crystal structure may be attributed to the need of geometric matching and minimizing energy within the crystal.

3.2. Thermal Behavior and Solid-State NMR Analysis. To compare the thermal behavior of the multicomponent crystals and their precursors, differential scanning calorimetry (DSC) was performed on the pure **A**, **B**, **C**, **A.B**, and **2A.C**(H_2O) crystals. For the pure precursors **A**, **B**, and **C**, the endotherms accompanying the melting endotherms appear at ca. 276, 144, and 244 °C, whereas endotherms of salts **A.B** and **2A.C** can be observed at 211.2 and 212.9 °C, respectively. These endotherms illustrate that the dissociation of **A.B** and **2A.C** occurs due to the difference in the melting points between TPI (high temperature) and its corresponding coformers **B** and **C** (low temperature). This phenomenon further shows that the hydrogen-bond interactions in the salts **A.B** and **2A.C** are stronger than those in pure **B** and **C** organic solids. Moreover, thermogravimetric analysis (TGA) profiles of crystal **A.B** and **2A.C**(H_2O) are shown in Figure 3. The shape weight losses occurring near the melting temperatures are assigned to the sublimation and/or decomposition process of the coformers within the multicomponent crystals, which further confirm the content ratios of the coformers to **A** (1:1 or 2:1) within the salts. For salt **A.B**, TGA shows a weight loss of ca. 49.4%, which occurs at 211 °C, this corresponds to the expected percentage content (50.3%) of coformer **B** in the **A.B** salt with a 1:1 ratio of **A** to **B**. For salt **2A.C**(H_2O), the first step weight loss of ca. 4.5% can be assigned to the loss of guest water molecules (theoretical value: 4.4%) within the host matrix **2A.C**; the second step is the weight loss (25.7%) of the coformer **C**, which is also consistent with the percentage content (23.2%) of coformer **C** in the **2A.C**(H_2O).

Solid-state ^{13}C and ^{15}N NMR were performed on both the pure **A** and as-obtained multicomponent organic crystals. For pure **A**, the resonances of the C_1, C_2, C_3, and C_4 in the phenyl group appear at 124.3, 126.6, 128.0, and 130.1 ppm, and those of C_5, C_6, and C_7 in the imidazole group are located at 135.4, 136.7, and 148.1 ppm respectively. In the **A.B** system, new peaks occurring at 120.6, 121.7, 142.9, and 161.6 ppm can be attributed to C_8, C_9, and C_{10} in the benzene as well as C_{11} in the carboxylate group of **B**. Moreover, the C_2 and C_3 peaks in the **A.B** sample are shifted downfield by 0.5 and 0.8 ppm compared with the pure **A** sample. Upon formation of the **2A.C**(H_2O), new peaks appear at 143.0 and 162.2 ppm, which can be assigned to the C_{12} and C_{13} in **C** as shown in the inset of Figure 4a. In addition, C_2 (127.2 ppm) and C_3 (128.6 ppm) peaks show a downfield shift of 0.6 ppm relative to those of pure **A**, suggesting that the coformers **B** and **C** containing fluorine atoms can polarize and delocalize the electronic density of the TPI molecule to some extent. Furthermore, resonances in the ^{15}N CP-MAS ssNMR spectrum of the pure **A** appeared

dx.doi.org/10.1021/cg3014927 | Cryst. Growth Des. 2013, 13, 333−340

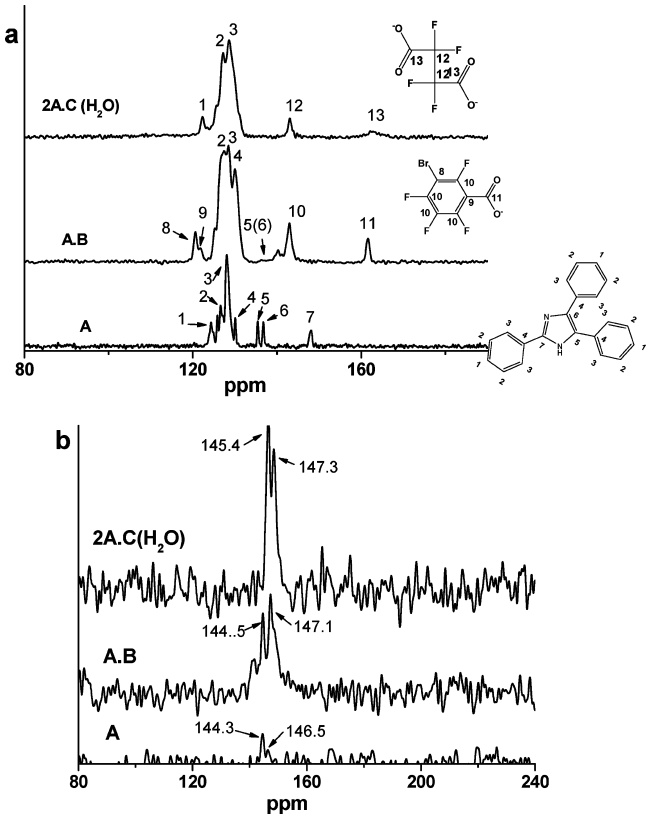

Figure 4. Solid ^{13}C (a) and ^{15}N NMR (b) profiles for both the pure **A** and as-obtained salts **A.B** and **2A.C**(H_2O).

at 144.3 and 146.5 ppm as shown in Figure 4b, which correspond to the nitrogen atoms with N−H and N···H fashions in the TMP crystal structure. After the occurrence of the assembly of **A** with **B** and **C**, two peaks move downfield to 144.5, 147.1, and 145.4, 147.3 ppm respectively. This illustrates the formation of two types of H-bonding in the N···H units of **A.B** and **2A.C**(H_2O).

3.3. Photophysical Properties. Figure 5 shows the excitation and emission spectra of pure **A**, **A.B**, and **2A.C**(H_2O) salts, respectively. For the pure **A** sample, the maximum excitation and emission wavelengths (λ_{ex}^{max} and λ_{em}^{max}) are located at ca. 349 and 382 nm, respectively. Upon formation of salts **A.B** and **2A.C**(H_2O), the λ_{ex}^{max} and λ_{em}^{max} are red-shifted systematically at 370, 362 and 387, 393 nm, respectively. The change in the photophysical properties of these organic solid compositions can be partially assigned to alternative arrangement of the molecules of **A** from the staggered pattern in pure **A** to antisymmetric parallel mode in the **A.B** and **2A.C**(H_2O). This behavior further suggests that the formation of the multicomponent crystals can alter the light emission behaviors of the pure organic chromophores. To obtain an insight into the excited-state information of fluorescence for these solids, the fluorescence lifetimes were measured and the corresponding fluorescence decay curves are shown in Figure 6. The fluorescence lifetimes were obtained by

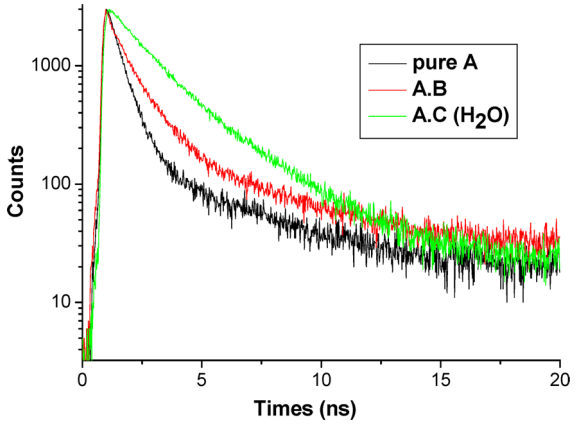

Figure 6. Fluorescence decay curves of the pure TPI (**A**) and salts (**A.B** and **2A.C**(H_2O)).

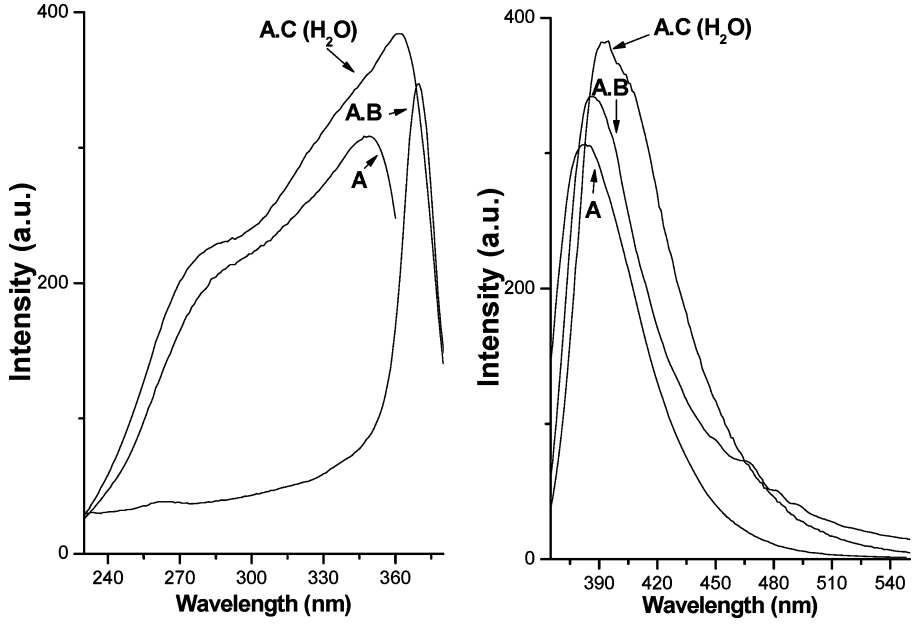

Figure 5. Fluorescence excitation and emission spectra for pure TPI (**A**) and salts (**A.B** and **2A.C** (H_2O)).

dx.doi.org/10.1021/cg3014927 | Cryst. Growth Des. 2013, 13, 333−340

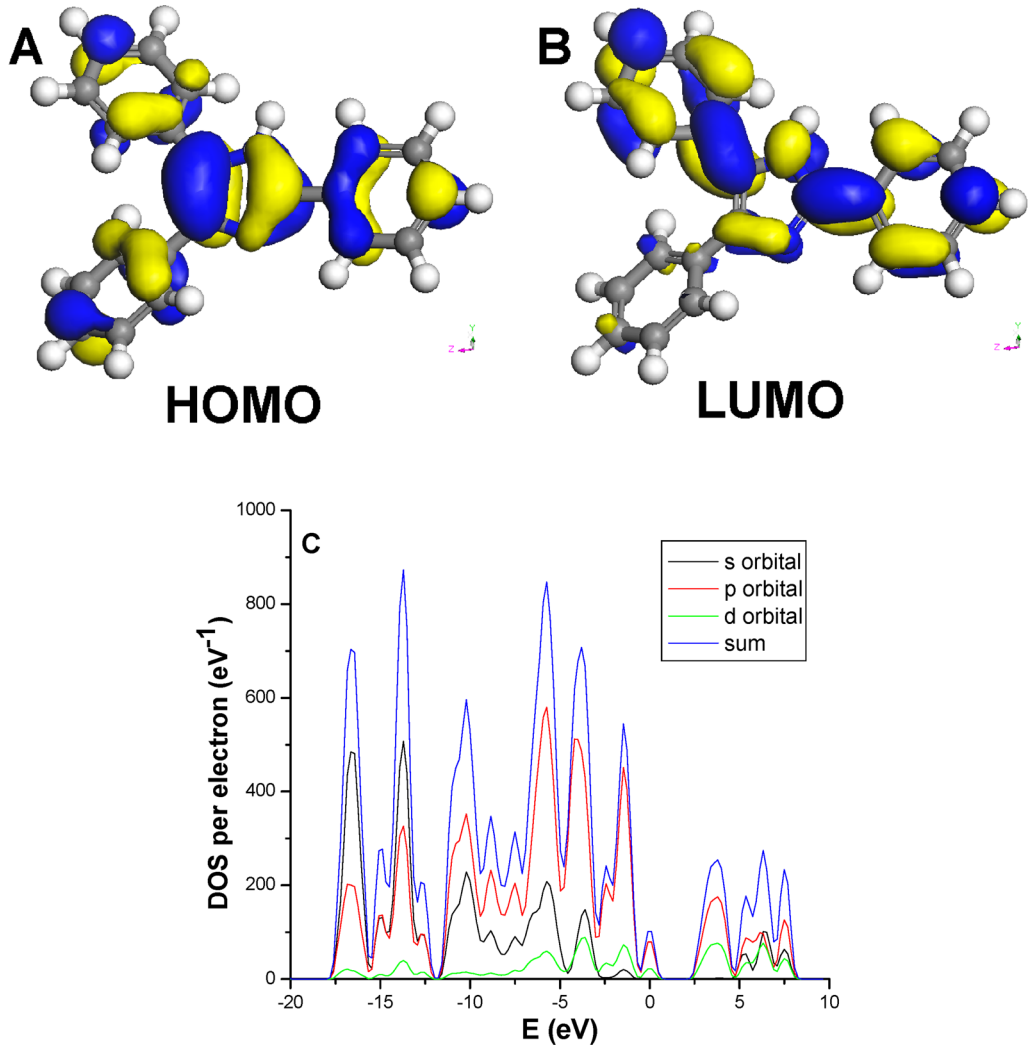

Figure 7. (A) HOMO, (B) LUMO, and (C) total and partial electronic density of states (TDOS and PDOS) profiles for pure **A** molecule. The Fermi energy level E_F was set to zero.

fitting the decay profiles with one-exponential form. The fluorescence lifetime of pure **A** with low-wavelength emission is 0.63 ns, whereas for **A.B** and **2A.C(H_2O)** salts with long-wavelength emission the values are 1.17 and 2.05 ns, suggesting that the formation of the multicomponent crystal can adjust the luminescent excited-state properties of the pure chromophore effectively. The enhancement of the fluorescence lifetimes can be attributed to the deformation of the TPI aggregation by the introduction of the coformers within the salts **A.B** and **2A.C(H_2O)**, which is consistent with the red-shift of the emission spectra for the salt samples. To detect the fluorescence efficiency of the samples, photoluminescence quantum yield (PLQY) was further measured. It was observed that PLQY values are 10.2%, 10.9%, and 15.1% for pure **A**, **A.B**, and **2A.C(H_2O)**, respectively. Such observation is also consistent with the trend of their fluorescence lifetime.

3.4. Periodic Density Functional Theoretical Calculations. To obtain energy level and electronic structural information of the TPI-based multicomponent systems, periodic density functional theoretical (DFT) calculations were performed on an individual molecule of **A**, a crystal of **A**, and salts **A.B** and **2A.C(H_2O)**. For the pure **A** molecule, frontier orbital analysis (Figure 7C and Figure S2 in the Supporting Information) shows that the electron densities of the highest occupied molecular orbitals (HOMOs) and lowest unoccupied molecular orbitals (LUMOs) are mainly located on the C and N atoms, and distributed over the whole π-conjugated **A** molecule (shown in Figures 7A and 7B). Similar results can also be obtained for the **A** crystal (Figure S3 in the Supporting Information), which indicates that the photoexcitation/emission processes for the **A** crystal involve the same mechanism as the free **A** molecule, and no intermolecular energy transfer appears during the photoexcitation/emission process as shown in Figure S4 in the Supporting Information. For both **A.B** and **2A.C(H_2O)**, total electronic densities of states (TDOS) and partial electronic densities of states (PDOS) analyses show that HOMOs are mainly populated on the **A** molecule, while LUMOs are located on both the C and N atoms in the **A** molecule and C atoms in its coformer **B** and F atoms in **C** respectively (Figure 8C and Figures S5C, S6, and S7 in the Supporting Information), which can also be viewed directly in Figure 8A,B and Figures S5A and S5B in the Supporting Information. These results show that the introduction of different coformers can influence the frontier orbital distribution and electronic structure in these multicomponent crystals, which can further influence the luminescent properties of the TPI-based organic solids as shown in the Experimental Section.

dx.doi.org/10.1021/cg3014927 | *Cryst. Growth Des.* 2013, 13, 333−340

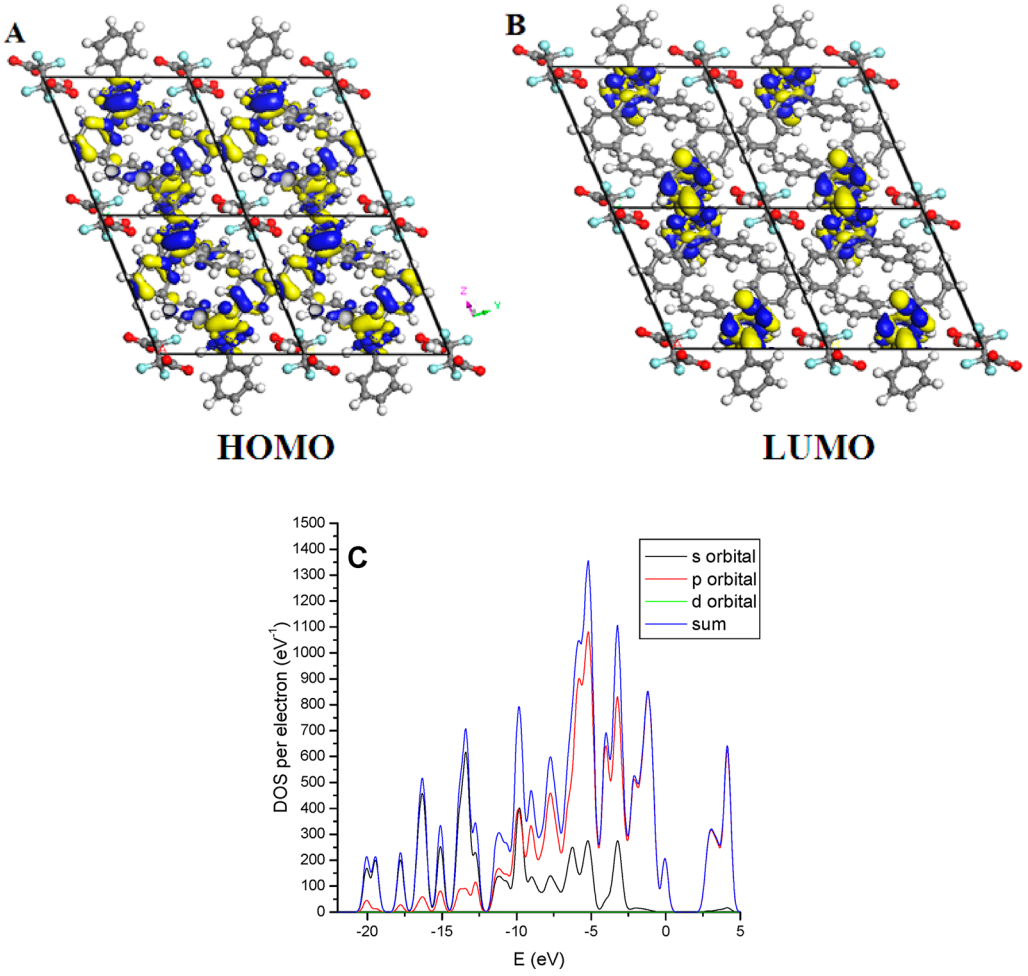

Figure 8. (A) HOMO, (B) LUMO, and (C) total and partial electronic density of states (TDOS and PDOS) profiles for **2A.C(H_2O)** salts. The Fermi energy level E_F was set to zero.

4. CONCLUSION

In summary, TPI-based multicomponent crystals have been synthesized by the use of mechanochemical methods. The molecular arrangement transfers from a staggered pattern in pure TPI crystal to an antisymmetric parallel arrangement between two adjacent TPI molecules in the salts due to the formation of the N−H···O hydrogen-bonding between TPI and its coformers. Compared with the pure TPI crystal, the two salts exhibit red-shift emission and enhanced fluorescence lifetime, which demonstrates that the optical properties in an organic solid chromophore can be adjusted and modulated by multicomponent crystal formation. Of particular interest here is the introduction of coformers to change the electronic structures and orbital distributions of the chromophore in the multicomponent crystals, which was confirmed by DFT calculations. It can be expected that the strategy of multicomponent crystal formation can be extended to tune the fluorescent properties of other organic chromophore systems for developing new types of organic luminescent materials.

■ ASSOCIATED CONTENT

Supporting Information

Profiles for the morphology of the salt crystals (Figure S1). Total and partial electronic density of states (TDOS and PDOS) profiles for different atoms in pure TPI (**A**) (Figure S2); HOMO/LUMO and TDOS/PDOS profiles for pure **A** crystal (Figure S3); TDOS and PDOS profiles for different atoms in pure **A** crystal (Figure S4); HOMO, LUMO and TDOS/PDOS profiles for **A.B** salt (Figure S5); TDOS and PDOS profiles for different atoms in **A.B** salt (Figure S6); TDOS and PDOS profiles for different atoms in **2A.C(H_2O)** salt (Figure S7); crystallographic data (.cif) of **A.B** and **2A.C(H_2O)** systems. This material is available free of charge via the Internet at http://pubs.acs.org.

■ AUTHOR INFORMATION

Corresponding Author

*E-mail: yandongpeng001@163.com; yandp@mail.buct.edu.cn. Fax: +86-10-64425385. Tel: +86-10-64412131.

Notes

The authors declare no competing financial interest.

■ ACKNOWLEDGMENTS

This work was supported by the National Natural Science Foundation of China, the 973 Program (Grant No. 2011CBA00504), and the 111 Project (Grant No. B07004). EPSRC and INTERREG IVA 2 Mers Seas Zeeën Cross-border Cooperation Programme 2007-2013 (BP) are acknowledged. Pfizer Institute of Pharmaceutical Materials Science is acknowledged for providing fellowship for AD.

REFERENCES

(1) (a) Xie, Z.; Yang, B.; Cheng, G.; Liu, L.; He, F.; Shen, F.; Ma, Y.; Liu, S. *Chem. Mater.* **2005**, *17*, 1287. (b) Schiek, M.; Balzer, F.; Al-Shamery, K.; Lützenc, A.; Rubahn, H.-G. *Soft Matter* **2008**, *4*, 277. (c) Yan, D. P.; Lu, J.; Wei, M.; Han, J. B.; Ma, J.; Li, F.; Evans, D. G.; Duan, X. *Angew. Chem., Int. Ed.* **2009**, *48*, 3073. (d) Yan, D. P.; Lu, J.; Wei, M.; Qin, S. H.; Chen, L.; Zhang, S. T.; Evans, D. G.; Duan, X. *Adv. Funct. Mater.* **2011**, *21*, 2497. (e) Strassert, C. A.; Chien, C.-H.; Lopez, M. D. G.; Kourkoulos, D.; Hertel, D.; Meerholz, K.; De Cola, L. *Angew. Chem., Int. Ed.* **2011**, *50*, 946. (f) Anthony, S. P.; Draper, S. M. *J. Phys. Chem. C* **2010**, *114*, 11708. (g) Lee, J. H.; Yuan, Y. Y.; Kang, Y. J.; Jia, W. L.; Lu, Z. H.; Wang, S. N. *Adv. Funct. Mater.* **2006**, *16*, 681.

(2) (a) He, F.; Tian, L. L.; Tian, X. Y.; Xu, H.; Wang, Y. H.; Xie, W. J.; Hanif, M.; Xia, J. L.; Shen, F. Z.; Yang, B.; Li, F.; Ma, Y. G.; Yang, Y. Q.; Shen, J. C. *Adv. Funct. Mater.* **2007**, *17*, 1551. (b) Zang, L.; Che, Y.; Moore, J. S. *Acc. Chem. Res.* **2008**, *41*, 1596.

(3) (a) Hara, K.; Kurashige, M.; Ito, S.; Shinpo, A.; Suga, S.; Sayamaa, K.; Arakawa, H. *Chem. Commun.* **2003**, 252. (b) Horiuchi, T.; Miura, H.; Sumioka, K.; Uchida, S. *J. Am. Chem. Soc.* **2004**, *126*, 12218. (c) Hong, Y.; Lam, J. W. Y.; Tang, B. Z. *Chem. Soc. Rev.* **2011**, *40*, 5361.

(4) (a) Fei, Z.; Kocher, N.; Mohrschladt, C. J.; Ihmels, H.; Stalke, D. *Angew. Chem., Int. Ed.* **2003**, *42*, 783. (b) An, B.-K.; Gihm, S. H.; Chung, J. W.; Park, C. R.; Kwon, S.−K.; Park, S. Y. *J. Am. Chem. Soc.* **2009**, *131*, 3950. (c) Zhang, X.; Rehm, S.; Safont-Sempere, M. M.; Würthner, F. *Nat. Chem.* **2009**, *1*, 623. (d) Li, C.; Zhang, Y.; Hu, J.; Cheng, J.; Liu, S. *Angew. Chem., Int. Ed.* **2010**, *49*, 5120. (e) Yan, D. P.; Lu, J.; Ma, J.; Qin, S.; Wei, M.; Evans, D. G.; Duan, X. *Angew. Chem., Int. Ed.* **2011**, *50*, 7175. (f) Feng, J.; Tian, K.; Hu, D.; Wang, S.; Li, S.; Zeng, Y.; Li, Y.; Yang, G. *Angew. Chem., Int. Ed.* **2011**, *50*, 8072. (g) Sagara, Y.; Kato, T. *Angew. Chem., Int. Ed.* **2011**, *50*, 9128. (h) Sagara, Y.; Kato, T. *Nat. Chem.* **2009**, *1*, 605. (i) Gu, X.; Yao, J.; Zhang, G.; Yan, Y.; Zhang, C.; Peng, Q.; Liao, Q.; Wu, Y.; Xu, Z.; Zhao, Y. S.; Fu, H.; Zhang., D. *Adv. Funct. Mater.* **2012**, *22*, 4862.

(5) (a) Nishiguchi, N.; Sato, T.; Kinuta, T.; Kuroda, R.; Matsubara, Y.; Imai, Y. *Cryst. Growth Des.* **2011**, *11*, 827. (b) Mizobe, Y.; Tohnai, N.; Miyata, M.; Hasegawa, Y. *Chem. Commun.* **2005**, 1839. (c) Yan, D.; Delori, A.; Lloyd, G. O.; Patel, B.; Friščić, T.; Day, G. M.; Bučar, D.-K; Jones, W.; Lu, J.; Wei, M.; Evans, D. G.; Duan, X. *CrystEngComm* **2012**, *14*, 5121. (d) Gao, H.; Shen, Q.; Zhao, X.; Yan, X.; Pang, X.; Jin, W. *J. Mater. Chem.* **2012**, *22*, 5336. (e) Shen, Q.; Wei, H.; Zou, W.; Sun, H.; Jin, W. *CrystEngComm* **2012**, *14*, 1010.

(6) (a) Desiraju, G. R. *Angew. Chem.Int. Ed.* **1995**, *34*, 2311. (b) Nangia, A. *Cryst. Growth Des.* **2008**, *8*, 1079. (c) Wuest, D. J. *Nat. Chem.* **2012**, *4*, 74.

(7) (a) Anthony, S. P.; Varughese, S.; Draper, S. M. *Chem. Commun.* **2009**, 7500. (b) Collas, A.; De Borger, R.; Amanova, T.; Blockhuys, F. *CrystEngComm* **2011**, *13*, 702. (c) Yan, D.; Delori, A.; Lloyd, G. O.; Friščić, T.; Day, G. M.; Jones, W.; Lu, J.; Wei, M.; Evans, D. G.; Duan, X. *Angew. Chem., Int. Ed.* **2011**, *50*, 12483. (d) Zhang, J.; Geng, H.; Virk, T. S.; Zhao, Y.; Tan, J.; Di, C.-A.; Xu, W.; Singh, K.; Hu, W.; Shuai, Z.; Liu, Y.; Zhu, D. *Adv. Mater.* **2012**, *24*, 2603. (e) Sato, S.; Nikawa, H.; Seki, S.; Wang, L.; Luo, G. F.; Lu, J.; Haranaka, M.; Tsuchiya, T.; Nagase, S.; Akasaka, T. *Angew. Chem., Int. Ed.* **2012**, *51*, 1589. (f) Landenberger, K. B.; Matzger, A. J. *Cryst. Growth Des.* **2010**, *10*, 5341. (g) Deng, Z.-P.; Huo, L.-H.; Zhao, H.; Gao, S. *Cryst. Growth Des.* **2012**, *12*, 3342. (h) Cavallo, G.; Aakeröy, C. B.; Champness, N. R.; Janiak, C. *CrystEngComm* **2010**, *12*, 22. (i) Luo, J.; Li, L.; Song, Y.; Pei, J. *Chem.—Eur. J.* **2011**, *17*, 10515. (j) Dong, B.; Wang, M.; Xu, C.; Feng, Q.; Wang, Y. *Cryst. Growth. Des.* **2012**, *12*, 5986.

(8) (a) Zhao, Y. S.; Yang, W.; Xiao, D.; Sheng, X.; Yang, X.; Shuai, Z.; Luo, Y.; Yao., J. *Chem. Mater.* **2005**, *17*, 6430. (b) Zhao, Y. S.; Xiao, D.; Yang, W.; Peng, A.; Yao, J. *Chem. Mater.* **2006**, *18*, 2302. (c) Zhao, Y. S.; Fu, H.; Hu, F.; Peng, A.; Yang, W.; Yao, J. *Adv. Mater.* **2008**, *20*, 79. (d) Liao, Q.; Fu, H.; Wang, C.; Yao, J. *Angew. Chem., Int. Ed.* **2011**, *50*, 4942. (e) Zhang, C.; Yan, Y.; Jing, Y. Y.; Shi, Q.; Zhao, Y. S.; Yao, J. *Adv. Mater.* **2012**, *24*, 1703.

(9) (a) Papaefstathiou, G. S.; Zhong, Z.; Geng, L.; MacGillivray, L. R. *J. Am. Chem. Soc.* **2004**, *126*, 9158. (b) Friščić, T.; Jones, W. *Cryst. Growth. Des.* **2009**, *9*, 1621. (c) Cinčić, D.; Friščić, T.; Jones, W. *Chem. Mater.* **2008**, *20*, 6623.

(10) Delley, B. *J. Chem. Phys.* **2000**, *113*, 7756.

(11) *Dmol3 Module, MS Modeling*, Version 2.2; Accelrys Inc.: San Diego, CA, 2003.

(12) Perdew, J. P.; Chevary, J. A.; Vosko, S. H.; Jackson, K. A.; Pederson, M. R.; Singh, D. J.; Fiolhais, C. *Phys. Rev. B* **1992**, *46*, 6671.

(13) Etter, M. C. *Acc. Chem. Res.* **1990**, *23*, 120.